Article

Iron Oxide and Hydroxide Speciation in Emissions of Brake-Wear Particles from Different Friction Materials using X-ray Absorption Fine Structure

Hiroyuki Hagino * , Ayumi Iwata , Tomoaki Okuda

Posted Date: 13 December 2023

doi: 10.20944/preprints202312.0786.v1

Keywords: brake dust; particulate matter; airborne particles; XAFS analysis; non-exhaust emissions

Article

Iron Oxide and Hydroxide Speciation in Emissions of Brake-Wear Particles from Different Friction Materials using X-ray Absorption Fine Structure

Hiroyuki Hagino [1,*], Ayumi Iwata [2,3] and Tomoaki Okuda [2]

[1] Japan Automobile Research Institute (JARI), 2530 Karima, Tsukuba, Ibaraki 305-0822 Japan 1; hhagino@jari.or.jp
[2] Faculty of Science and Technology, Keio University, 3-14-1, Hiyoshi, Yokohama 223-8522, Japan
[3] Meteorological Research Institute Japan Meteorological Agency, 1-1 Nagamine, Tsukuba, Ibaraki 305-0052, Japan
* Correspondence: Author to whom correspondence should be addressed.

Abstract: Iron (Fe), the main component of non-exhaust particulates, is known to have variable health effects that depend on the chemical species of iron. This study characterized the possible contribution of iron oxides and hydroxides to airborne brake-wear particles under realistic vehicle driving and braking conditions with different brake-pad friction materials. We found significant differences in wear coefficients and PM_{10} emissions between non-asbestos organics (NAO) and European performance (ECE) brake pads. Iron was the dominant contributor to PM_{10} and $PM_{2.5}$ brake-wear particles for both NAO and ECE. The iron concentration ratio in the particle mass were comparable to the disc to pads ratio measured by wear mass. The fact that magnetite, which is of interest with respect to health effects, was less abundant in NAO than in ECE suggested that tribo-oxidations occurred in NAO. Metallic iron is generated not only from abrasive wear but also from tribo-chemical reduction with magnetite as the starting material. We found differences not only in PM emissions between brake friction materials but also that the phase transformations of iron differed between friction materials. These differences were apparent in the distribution of iron oxides and hydroxides. Heat, tribo-oxidation, and tribo-reduction are intricately involved in these reactions.

Keywords: brake dust; particulate matter; airborne particles; XAFS analysis; non-exhaust emissions

1. Introduction

Exposure of humans to particulate matter due to air pollution is associated with a range of respiratory, cardiovascular and neurological problems that are known to cause increased morbidity and mortality worldwide [1]. Particulate matter is known to be a complex mixture of organic and inorganic components emitted from a variety of primary sources and subject to various types and degrees of secondary reprocessing and environmental weathering. Exhaust particles consisting of carbonaceous compounds are a major source of air pollution from particulate matter in urban areas, but as emission controls reduce combustion-derived exhaust particles [2], the proportion of non-exhaust particles in particulate matter likely to be inhaled by humans in urban areas and near road traffic will increase. The most abundant element in non-exhaust particulates is generally known to be iron (Fe). In particular, its presence in wear products from vehicle braking systems and in engine emissions from combustion and/or wear suggests that urban traffic is an important source of Fe in particulate matter in urban areas [3]. Identification of the source of Fe in urban areas has revealed that the wear of Fe on brake pads containing steel fibers or Fe powder and grey cast iron discs has been a source of metallic Fe (Fe (0)) [4–8]. Magnetite (Fe_3O_4, Fe (II,III)) nanoparticles with a particle size of less than 100 nm are thought to be introduced into urban air from vehicle exhaust emissions, engine wear, and braking system wear [4,6,7]. The oxides and hydroxides of Fe (e.g., metallic iron (α-Fe, Fe (0)); divalent iron (Fe (II)); and trivalent iron (Fe (III)) may play an important role in the development of neurodegeneration and Alzheimer's disease e.g., [9]. It is therefore important to be

 doi:10.20944/preprints202312.0786.v1

able to distinguish the iron oxides and hydroxides in order to identify the contribution of sources of non-exhaust particles in urban areas by iron speciation as well as the potential impact on human health due to iron particles.

Braking systems for motor vehicles are known to be an important source of iron in non-exhaust particulates in urban areas, and they vary according to the type of vehicle as well as the national and regional markets. Brake pads in the basic brake system of a modern car are available in a wide range of compositions of friction material, with the gray cast iron brake disc also regarded as a component of the friction material. The two most important categories are low-steel (low metallic) pads (also called "ECE"), developed and produced primarily for the European market, and non-asbestos organic (NAO) pads, designed primarily for the North American and Asian markets [10]. These two material concepts can be distinguished, inter alia, by the percentage of metal components. Low steel (low metallic) pads contain a significant percentage of iron, whereas NAO pads are usually iron-free.

Brake disc and pad wear products include brake-wear particles and the subsequent formation of friction layers. Brake-wear particles and gases are released from surfaces of pads and disc [4]. The brake-wear particles adhere to the friction surface of the brake pad and form a friction layer. This layer is critical to the ability of each brake pad to function as a source of friction. Iron oxide has proven to be the main component of the friction layer [11]. For example, dynamometer tests have been performed with ECE brake material at different temperatures from 25 to 700°C. At temperatures above 400°C, the formation of magnetite (Fe_3O_4, Fe (II, III)) and maghemite (γ-Fe_2O_3, Fe (III)) has been detected, and above 600°C, the formation of hematite (α-Fe_2O_3, Fe (III)) has been detected. Lepidocrocite (γ-Fe(O)OH, Fe (II)) formation has been detected only at 400°C [12]. In contrast, pin-on-disc tests of NAO brake materials with maximum achieved contact temperatures below 50°C have been performed, and magnetite (Fe_3O_4, Fe (II, III)), a product of tribo-oxidation of cast iron discs, has been reported to be the principal mineral formed on the friction layer [13]. Because different magnetite (Fe_3O_4, Fe (II, III)) formation temperatures have been reported, the friction phenomena are complex, and the mechanism of formation of the friction layer is not yet fully understood, even though the wear particle structures present on the brake pad surface are very important in terms of brake-wear particle emissions [4]. There is very limited knowledge of iron speciation of airborne brake-wear particles from various brake friction materials of relevance to air quality and human health. Tests have been conducted under braking conditions such as the Worldwide-harmonized Light Vehicle Test Procedure Brake Cycle [14].

The goal of this study was therefore to characterize the possible contribution of iron oxides and hydroxides to airborne brake-wear particles under realistic vehicle driving and braking conditions with different friction materials. Iron chemical forms were identified using the X-ray absorption fine structure (XAFS) method [15,16] in order to allow bulk measurements in any solid or liquid state regardless of the sample phase, to avoid the influence of iron magnetism [7] and to reduce the cumbersome analytical operations that contribute to measurement errors.

2. Materials and Methods

2.1. Brake Dynamometer Test and Airborne Brake-wear Particle Measurement

Brake-wear particles were measured and collected in accord with a previous study [17] and the JASO C 470 test protocol [18]. A single passenger car front brake wheel was used for driving and brake control in accord with the worldwide light vehicle test procedure (WLTP) brake driving profile [19] using an electric inertia dynamometer. The test brake assembly was a commercially available genuine brake assembly; it consisted of a cast iron ventilated disc, floating caliper, and brake pads made of NAO material or ECE (European performance brake pads) materials, and the elements it contained were measured by wavelength-dispersive X-ray fluorescence analysis (ZSX Primus II, Rigaku, Corp.). Disc temperature was measured by locating a thermocouple 10 mm radially outward from the center of the friction pad and at a depth of 1.0 ± 0.1 mm from the disc surface.

Two pad types were tested with individual conventional gray cast iron brake discs of the same type. The NAO and ECE tests were conducted on cast iron discs of each material, and the WLTP

brake cycle was repeated three times after bedding in accord with the JASO C470 test protocol [18]. The test vehicle mass was 1240 kg, and the brake force front/rear distribution was 80%, with a tire dynamic load radius of 298 mm, an inertia of 38.3 kg-m^2, and a wheel load to disc mass (WL/DM) ratio [20] of 69.3. Because the Global Technical Regulation (GTR24) test method was not defined at the time of this experiment [20], the sampling of brake-wear particles was based on the JASO C 470 test method, which consists of an enclosure with the brake assembly inserted downstream of the air supplied through an HEPA filter and a constant-flow sampling tunnel (1 m^3/min, 20°C standard) [18]. Sampling of PM_{10} and $PM_{2.5}$ were carried out with a low-pressure impactor (LPI) (LP-20, Tokyo Dylec Corp.) according to the methods previous reported [17] on a Teflon filter (Filter A; Fluoropore FP-500-100, 47 φ for PM_{10} and $PM_{2.5}$, 80 φ for LPI, Sumitomo Electric Fine Polymer Corp.), (Filter B; Teflo®, 47 φ for PM_{10} and $PM_{2.5}$, Pall Corp.) or a quartz filter (Pallflex®, 2500QAT-UP, 47 φ for PM_{10} and $PM_{2.5}$, Pall Corp.) by aspirating from a sampling nozzle equipped with isokinetic sampling nozzles. Filter masses before and after the test were weighed on an electronic balance to determine the emissions of PM_{10} and $PM_{2.5}$. A cyclone particle collector (a sanitary stainless-steel cyclone with electropolished interior, Clean Valve Co. Ltd.) was installed at the end of the constant flow sampling tunnel to collect PM_{10} powdered brake-wear particles. The diameters of the particles collected by the cyclone were at least 100 nm, which is the same geometry as in previous studies with a PM_{10} impactor (HV-1000-PM10, Shibata Scientific Technology Ltd.) attached to the cyclone inlet [21,22]. The cyclone sampling method for particulate matter in this study is also suggested as a method that can be used to assess health effects e.g., [23], as it is a technique that collects particles in the air as a powder. Organic and elemental carbon (OCEC) were measured by a thermal-optical carbon analyzer (model 2001, Desert Research Institute) using the IMPROVE protocol [24]. Total metals, including water-soluble and insoluble fractions, were measured via energy dispersive X-ray fluorescence (XRF) (Epsilon 5, Malvern PANalytical) [25].

2.2. X-ray Absorption Fine Structure Analysis

To identify the iron speciation in the brake-wear particles and to quantify their contribution, we used mainly X-ray absorption near edge structure (XANES) to study the valence state of absorbed atoms measured at the Kyushu Synchrotron Radiation Research Center (SAGA-LS) using beamlines 11 and 15 [15,16]. We ensured the quality of the continuous spectra through XAFS measurements using synchrotron radiation [16]. The analytical method is described in brief here.

Speciation of each metal compound was performed by a linear combination fitting method using metal reference compounds (Fe, FeO, Fe_3O_4, Fe_2O_3(α,γ), and Fe(O)OH). Each reference compound was mixed well with boron nitride in a mortar for 20 min and then pressed into pellets similar to the aerosol samples. A total of six PM_{10} powder samples (NAO and ECE) and four $PM_{2.5}$ filter samples were subjected to XAFS separation of the chemical forms of iron. XAFS spectra were measured in the energy region 6781–7858 eV near the Fe K-edge for each of the six standard and analyzed samples by the transmission method (I0, He 50%: N_2 50%; I1, N_2 85%: Ar 15%) for all the samples. The measurement parameters were set to 0.36 eV/step (1 s/step) only in the XANES region from 7081 to 7172 eV/step for all samples and 1.91 to 9.90 eV/step (1 s/step) for the remaining regions (12.6 min in total). The two PM_{10} powder samples and the Fe(O)OH reference sample to be analyzed, other than the SAGA-LS–owned reference sample, were weighed, and each powder was mixed using a pestle and mortar for 20 min, after which time the powder was pressed at 50 kN into a 13-mm diameter pellet mold and placed in plastic bags for measurement. Four filter samples were also placed in a plastic bag and measured in the same way.

For the XAFS spectrum analysis, normalization of the experimental data and the linear fitting calculation using the least-squares method for valence ratio were performed using Athena software (ver. 0.9.26) [26]. The detailed procedures are described in a previous study [15,16]. The R factors, which are generally used for the evaluation of fitting results, fell in the range 0.002–0.06 for iron speciation in the linear combination fitting analysis.

 doi:10.20944/preprints202312.0786.v1

3. Results and Discussion

3.1. Charactorization of Brake-wear Particles

3.1.1. Brake Pad and Disc Wear

The amounts of disc and brake pad wear (i.e., mass loss [20,27]) can provide information that facilitates evaluation of the reasonableness of the particulate matter measurements in this study compared to previous studies that measured brake-wear particles, which are known to have high variability. For mass loss measurement [27] in this study, the WLTP brake cycle was repeated three times after beddings to allow sufficiently accurate measurement of the wear mass, and the mass difference between the pad and disc before and after the test was measured. Mass loss of the NAO pads was 0.92 g for the pads (inner), 0.65 g for the pads (outer), and 0.75 g for the discs, for a total of 2.32 g. Brake-wear particles are known to result from wear of discs as well as brake pads. Disc wear accounted for 32% of the total wear. Mass loss as a wear factor was determined by dividing the total mass loss of the friction partner (mg) by the total test mileage (km) of the three tests. Mass loss was 4.02 mg/km per brake for the NAO pads in Figure 1. Mass loss for the ECE pads was 1.31 g for the pads (inner), 0.87 g for the pads (outer), and 3.19 g for the discs, for a total of 5.37 g. Disc wear accounted for 59% of the total wear. Mass loss as a wear factor was 9.31 mg/km per brake with ECE pads (Figure 1). A comparison of these results to the benchmarks of a previous interlaboratory study (ILS) [8] revealed that higher emissions were observed in that study than in this study, 6.5 mg/km per brake with NAO pads and 21 mg/km per brake with ECE pads [27,28]. NAO was developed to optimize comfort (reduction of noise and rim contamination), and this study (Figure 1) and previous studies have shown higher emissions with ECE than with NAO [27]. However, this comparison is based on different brake assemblies and masses of test vehicles, and in this study, we found higher wear coefficients with ECE in only some pairings of NAOs and ECEs with discs. Further systematic studies will be needed clarify whether there are significant differences in wear coefficients between NAO and ECE pads.

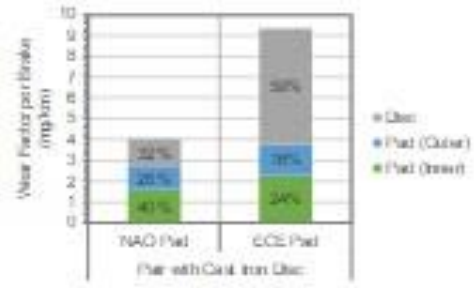

Figure 1. Comparison of NAO and ECE pads paired with conventional gray cast iron ventilated discs in wear coefficients for the front brake axle.

3.1.2. Brake-wear Particle Emissions

Emissions of brake-wear particles (average of n = 3) were 1.43 ± 0.29 (3.73 ± 0.19) mg/km per brake for PM_{10} and 0.59 ± 0.08 (1.31 ± 0.08) mg/km per brake for $PM_{2.5}$ with NAO (ECE). The PM_{10} to mass loss ratio [27] was 35% for the NAO pairing and 40% for the ECE pairing. In contrast to this result, a comparison of the results of previous studies by the authors, both using the same friction material (PV565 unique identification code based on brake friction registration by the National Sanitation Foundation), showed that the PM_{10} of Vehicle II in the literature [17] was 29% comparable to 35% for the NAO pairing of this study, although the test vehicle (mass 1240 kg, tire dynamic rolling radius 298 mm, 80% brake front-rear distribution), braking system, and driving conditions (JC08) were very different [17]. However, these results showed a slightly lower detection than those of the interlaboratory study [27], which reported the average PM_{10} to mass loss ratio for disc brake systems to be 35–49%. The fact that the average PM_{10}/mass loss ratio for disc brake systems in the interlaboratory study [27] fell in the range 35–49% suggested that the brake systems used in this study

Preprints (www.preprints.org) | NOT PEER-REVIEWED | Posted: 13 December 2023 doi:10.20944/preprints202312.0786.v1

lost weight for other reasons, such as adhesion to the calipers or scrub remaining on the pad surface during adhesive wear. It is therefore reasonable to assume that the PM_{10} to mass loss was not 100%, and that the ratio varies as a function of the friction material, disc material and structure, and caliper structure.

In this study, we measured the emissions of particle masses according to their aerodynamic particle diameters measured with a low-pressure impactor (LPI), and the results are shown in Figures 2. Generally, because the height of each particle size intervals is affected by the width of that intervals, which distorts the shape of the fraction, a histogram is used for the vertical axis, in which the particle mass of each fraction is divided by the width of that fraction (*dM/dlogDp*), and the particle size distribution is normalized by the particle size intervals [29]. However, in this study, the height of each particle size fraction is expressed as the emission factor of the particle mass measured in each fraction, so the vertical axis of the graph is used as *dM*. The emissions were distributed in the mode diameter range of 1–5 μm throughout the WLTP-Brake Cycle. The ratio of emissions of nanoparticles ($PM_{0.12}$ based on LPI specifications) to PM_{11} was 0.05% (0.0006 mg/km) for NAO and 0.06% (0.0015 mg/km) for ECE. For the brakes investigated in this study, the contributions of nanoparticles to the overall PM emissions were small. The implication is that even cyclones with low collection efficiencies for particles smaller than 0.1 nm generally collected all of the PM_{10} in this study.

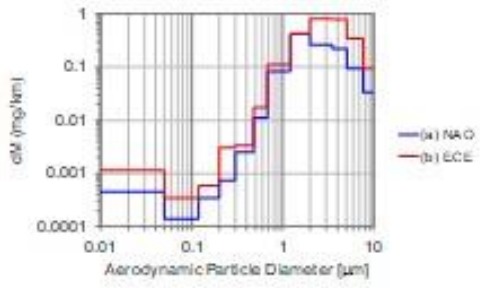

Figure 2. Particle mass size distributions of NAO and ECE paired with a conventional gray cast iron ventilated disc, as indicated by the coefficient of wear of the front brake axles.

3.1.3. Chemical Characterization

The brake-wear particle emissions test required in GTR24 addresses only physical quantities such as particle mass (PM_{10} and $PM_{2.5}$) and number of particles (total particle numbers and solid particle numbers) [20]. The composition of brake-wear particles can provide important information on air quality implications, mechanisms of toxicity, and mechanisms of brake-wear. Figure 3(a)–(f) show the elemental contents of the pad friction surface, PM_{10}, and $PM_{2.5}$ in NAO and ECE. Because the aim of this study was Fe speciation, this discussion will focus on Fe in Figure 3(a)–(f). Each of the NAO and ECE brake pads contained some iron (Figure 3(a) and (d), respectively), although NAOs is typically iron-free [10]. The NAO used in this study contained less iron than the ECE because this NAO was developed and produced for both the European and Asian markets. There are various types of NAOs, and the brake pads used in this study were NAOs according to the manufacturer. The contribution of Fe tends to increase from the pad (Figure 3(a) and (d)) to brake-wear particles (Figure 3(b), (c), (e), and (f)), and it is most abundant in PM_{10} and $PM_{2.5}$ for both NAO and ECE. The friction material counterpart, the cast iron disc, is composed mainly of iron and tiny amounts of additive metals. When the disc was ground by the pad, wear particles that contributed to the brake-wear particles (PM_{10} and $PM_{2.5}$) were emitted. These results support the findings of previous studies [17,30].

Preprints (www.preprints.org) | NOT PEER-REVIEWED | Posted: 13 December 2023 doi:10.20944/preprints202312.0786.v1

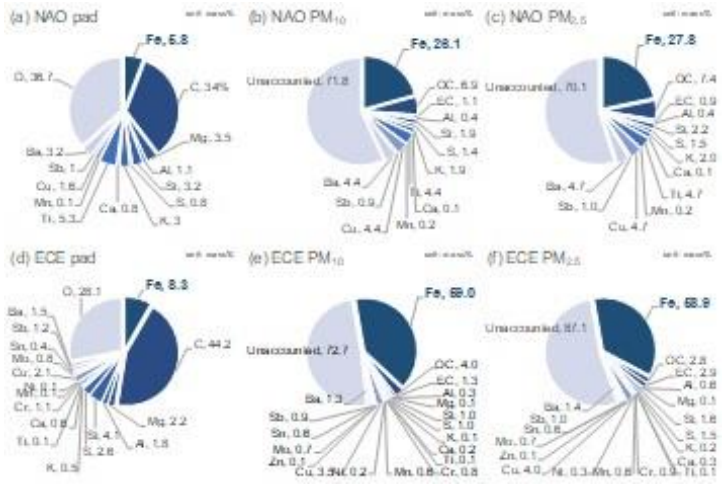

Figure 3. Elemental components of the pad friction surface, PM_{10}, and $PM_{2.5}$ in NAO and ECE paired with discs.

The PM originating from disk wear (PM_{disc}) and pad wear (PM_{pad}) can be distinguished from the PMx, where x equals 2.5 or 10, by solving the following simultaneous Equations (1) and (2), which express the PM and Fe mass balance:

$$PM_{disc} + PM_{pad} = PMx, \quad (1)$$

$$[Fe]_{disc} \times PM_{disc} + [Fe]_{pad} \times PM_{pad} = [Fe]_{PMx} \times PMx. \quad (2)$$

Here,

PMx: PM_{10} or $PM_{2.5}$ emissions,

$[Fe]_{disc}$: Fe mass concentration (%) in the disc fixed as 100%, and

$[Fe]_{pad}$: Fe mass concentration (%) in the pad.

The result for $[Fe]_{pad}$ was 5.8% and 8.3%, for NAO and ECE, respectively. By solving Equations (1) and (2), we determined the contribution of the disc to the PMx (F_{disc} [%]) from Equation (3):

$$F_{disc} = PM_{disc} / PMx \times 100 = ([Fe]_{PMx} - [Fe]_{pad}) / ([Fe]_{disc} - [Fe]_{pad}) \times 100. \quad (3)$$

From the elemental analysis of collected PM_{10} and $PM_{2.5}$, [Fe] we determined PMx in the NAO (ECE) to be 26.1% (59.0%) for PM_{10} and 27.8% (58.9%) for $PM_{2.5}$. We could therefore estimate the mass fraction of PM_x originating from the disk (F disk = PMdisc/PMx) (%) to be 22% (55%) in the NAO (ECE) for PM_{10} and 23% (55%) in the NAO (ECE) for $PM_{2.5}$. The percentages contributed by the disk to PM_{10} and $PM_{2.5}$ were generally consistent with and not contradictory to the results of the elemental analysis. The disc wear rates measured from mass loss in this study accounted for 32% of total wear for the NAO pairing and 59% for the ECE pairing, respectively. Although not all of the disc wear particles and debris deposited on the ground are emitted as PM_{10} or $PM_{2.5}$, the Fe concentrations in the PM measured in this study suggest that the iron concentration ratio for particle mass were comparable to the disc to pads ratio measured by wear mass.

3.2. Iron Speciation

3.2.1. XAFS Spectra for Reference Materials

For quantitative speciation of iron oxides and hydroxides, XAFS spectra were measured for a total of six chemical species: metallic Fe (α-Fe, Fe (0)) as the reference material for iron; two Fe(III) iron oxides, hematite (α-Fe_2O_3, Fe (III)) and Maghemite (γ-Fe_2O_3, Fe (III)), with different crystal structures; the iron oxide magnetite (Fe_3O_4, Fe (II, III)) with co-existing divalent and trivalent iron oxides; the divalent iron oxide wüstite (FeO, Fe (II)); and the trivalent iron hydroxide goethite (α-Fe(O)OH, Fe (III)). The results are shown in Figure 4(a)–(d).

Preprints (www.preprints.org) | NOT PEER-REVIEWED | Posted: 13 December 2023 doi:10.20944/preprints202312.0786.v1

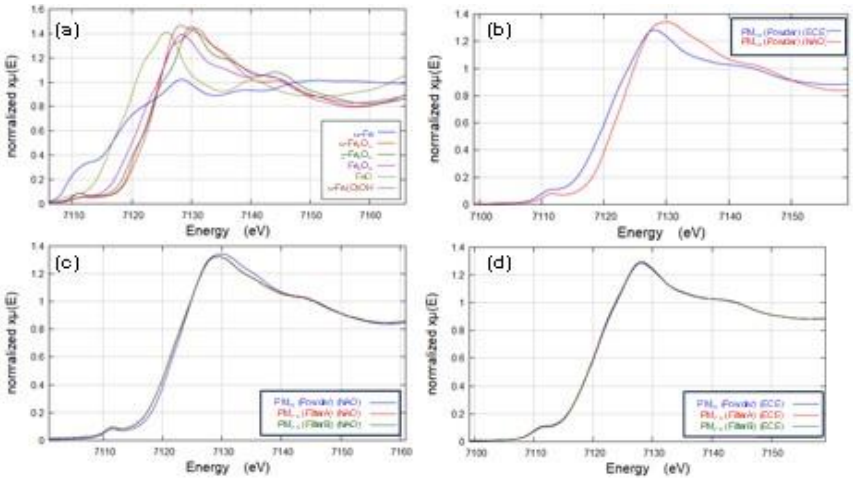

Figure 4. XAFS spectra of (a) standard samples, (b) NAO and ECE for powdered PM_{10} samples, (c) NAO for powdered PM_{10} and filtered $PM_{2.5}$ samples, and (d) ECE for powdered PM_{10} and filtered $PM_{2.5}$ samples.

The position of the absorption edge with the largest peak was basically different for each chemical species, but peaks were obtained in approximately the same energy region for the three species of metallic Fe (α-Fe, Fe (0)), magnetite (Fe_3O_4, Fe (II, III)), and goethite (α-Fe(O)OH, Fe (III)). The absorption edges of hematite (α-Fe_2O_3, Fe (III)) and Maghemite (γ-Fe_2O_3, Fe (III)) were also detected at similar positions for the iron oxide species hematite (α-Fe_2O_3, Fe (III)) and Maghemite (γ-Fe_2O_3, Fe (III)), but the highest peaks were shifted by about 1 eV. The fact that the spectrum of hematite (α-Fe_2O_3, Fe (III)) had a unique peak at about 7125–7130 eV suggested that the crystal structure could be distinguished. The same trivalent iron was also used as the crystal structure of hematite (α-Fe_2O_3, Fe (III)). The positions of the peaks differed between hematite (α-Fe_2O_3, Fe (III)) and goethite (α-Fe(O)OH, Fe (III)), even if they contained the same trivalent iron. It is therefore possible to distinguish chemical species with the same valence but different chemical states using this method. The clear differences between the XAFS spectra of each chemical species indicated that the present method was effective for identification of iron chemical species.

3.2.2. XAFS Spectra for Brake-wear Particles

Figure 4(b) shows the XAFS spectra of PM_{10} powder samples of NAO and ECE brake-wear particles. The fact that the shapes of the XAFS spectra of NAO and ECE were very different implies that the amounts of Fe in the two brake friction materials differed. Figure 4(c) and Figure 4(d) show the XAFS spectra of the PM_{10} powder and $PM_{2.5}$ filter samples of NAO and of ECE, respectively. ECE PM_{10} powder and filter samples yielded similar spectra that largely overlapped, whereas NAO PM_{10} powder and filter samples yielded spectra with slightly different shapes. These results suggested that the separation of the chemical form of iron in brake-wear particles was not affected by the collection method, the analytical form of the sample (powder and filter samples), or the particle size (PM_{10}, $PM_{2.5}$).

3.2.3. Iron Speciation

One goal of this research was to characterize and quantify the possible contributions of iron oxides and hydroxides to the airborne brake-wear particles under realistic vehicle driving and braking conditions with different friction materials. A number of hetero-iron compounds other than iron oxides and hydroxides have been detected in brake-wear particles [11–13]. This study focused exclusively on iron oxides and hydroxides, which have been detected in atmospheric observations [3,6] and discussed in terms of health effects [e.g., 9]. The iron oxides and hydroxides discussed in this study may therefore be an overestimation.

Preprints (www.preprints.org) | NOT PEER-REVIEWED | Posted: 13 December 2023 doi:10.20944/preprints202312.0786.v1

Figure 5 shows the results of our quantitative evaluation of the phase composition of brake-wear particles from emission measurements made on NAO and ECE.

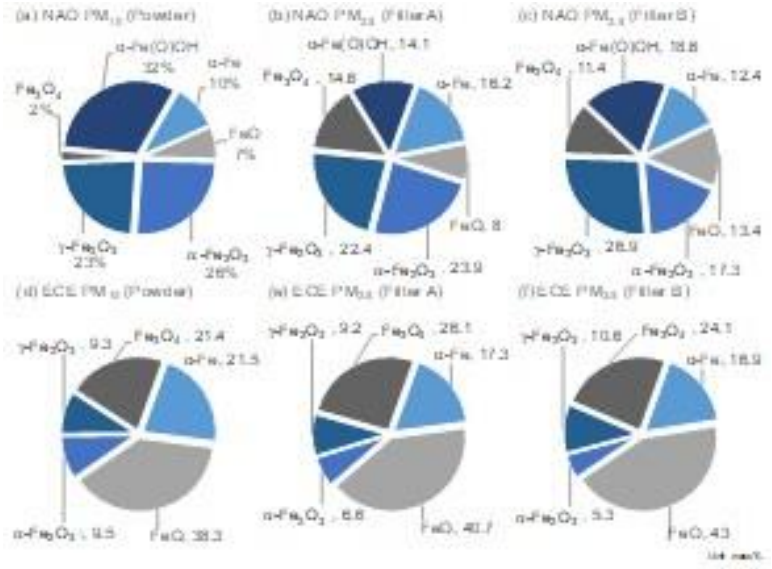

Figure 5. Iron speciation of (a) NAO of powdered PM_{10} samples, (b) NAO of powdered $PM_{2.5}$ samples (Filter A), (c) NAO of powdered $PM_{2.5}$ samples (Filter B), (d) powdered PM_{10} samples, (e) ECE of powdered $PM_{2.5}$ samples (Filter A), (f) ECE of powdered $PM_{2.5}$ samples (Filter B).

When we compared NAO (Figure 5(a)–(c)) and ECE (Figure 5(d)–(f)), we observed a higher proportion of the Fe (III) iron oxide Fe_2O_3 (sum of hematite (α-Fe_2O_3, Fe (III)), Maghemite (γ-Fe_2O_3, Fe (III))), and goethite (α-Fe(O)OH, Fe (III)) in NAO. Conversely, we observed a higher proportion of zero-valence metallic Fe (α-Fe, Fe (0)), divalent iron oxide wüstite (FeO, Fe (II)), and mixed divalent and trivalent iron oxide magnetite (Fe_3O_4, Fe (II, III)) in ECE. A comparison of the $PM_{2.5}$ filter samples obtained from the same brake as the NAO showed a common trend in that Fe_2O_3 (sum of hematite (α-Fe_2O_3, Fe (III)) and Maghemite (γ-Fe_2O_3, Fe (III))) accounted for about 45% in both cases. The remaining chemical species were present in the 10% range on average, although there were some differences. In the PM_{10} sample of NAO, the proportions of metallic Fe (α-Fe, Fe (0)), wüstite (FeO, Fe (II)), Fe_2O_3 (sum of hematite (α-Fe_2O_3, Fe (III)), and Maghemite (γ-Fe_2O_3, Fe (III))) were similar, whereas magnetite (Fe_3O_4, Fe (II, III)) was less abundant, and goethite (α-Fe(O)OH, Fe (III)) was detected more frequently. We thus observed that in the particles generated from this type of brake, there was a tendency for a large amount of magnetite (Fe_3O_4, Fe (II, III)) to be contained in the small particles with diameters less than 2.5 μm and a large amount of goethite (α-Fe(O)OH, Fe (III)) to be present in the coarse particles with diameters of 2.5 μm or more.

Next, a comparison of the composition of PM_{10} and $PM_{2.5}$ in the filter samples obtained from ECE showed that in both cases, wüstite (FeO, Fe (II)) accounted for more than 40% of the iron; Fe_2O_3 (sum of hematite (α-Fe_2O_3, Fe (III)) and Maghemite (γ-Fe_2O_3, Fe (III))) accounted for about 16%; goethite (α-Fe(O)OH, Fe (III)) was not detected; and we observed a low proportion of trivalent iron. For other chemical species, metallic Fe (α-Fe, Fe (0)) was observed at around 17%, and magnetite (Fe_3O_4, Fe (II, III)) was present at around 25% for both PM_{10} and $PM_{2.5}$. When $PM_{2.5}$ filter samples (different filters collected) of ECE were compared, there were some differences, but no significant overall differences in trends were observed for magnetite (Fe_3O_4, Fe (II, III)) for both PM_{10} and $PM_{2.5}$.

A previous study [6] has reported that the PM_{10} of brake-wear particles collected from a brake dynamometer using ECE contains about 20.2% magnetite (Fe_3O_4, Fe (II, III)), 1.6% metallic iron (Fe (0)), and 54.6% hematite (α-Fe_2O_3) (Fe (III)). The differences between the literature and this study for small percentages of metallic iron (Fe (0)) could be attributed to differences in the friction material of the ECE pads or to differences in the braking conditions, but the details are unknown. However, the distribution of the chemical forms of iron quantified in this study could be used as source profiles

Preprints (www.preprints.org) | NOT PEER-REVIEWED | Posted: 13 December 2023 doi:10.20944/preprints202312.0786.v1

and deployed to source apportionment study in atmospheric observations and thereby facilitate further research.

3.2.4. Phase Transformation

The important aspect of the above results (Figure 5) regarding the difference between NAO and ECE is that goethite (α-Fe(O)OH, Fe (III)) was not detected in ECE and contributed less to NAO $PM_{2.5}$ than to NAO PM_{10}. There are results of no goethite detected using ECE brakes and cast-iron discs [7] and results of minor goethite detected at low brake temperatures [8], respectively, supporting the result of almost no goethite in ECE in this study. On the other hand, a mixture of hydroxides, including goethite (α-Fe(O)OH), is also detected on the disc and pad surface as the main corrosion products of gray cast iron [31].

First, this study considered the phase transformation of iron oxides and hydroxides, since the ECE and NAO were collected at roughly the same time, with a difference in testing time of about one week, and not under conditions where iron is prone to corrosion in an excessively humidified atmosphere. The phase transformation of the iron oxides and hydroxides $Fe_xO_yH_z$ with temperature typically occurs at 675°C for hematite (α-Fe_2O_3, Fe (III)), <600°C for maghemite (γ-Fe_2O_3, Fe (III)), 575–586°C for magnetite (Fe_3O_4, Fe (II, III)), <575°C for wüstite (FeO, Fe (II)), and <200°C for goethite (α-Fe(O)OH, Fe (III)) [32,33], although there are some differences that depend on the particle size. The temporal profiles of the disc temperatures shown in Figure 6 indicate that the difference between ECE brake temperatures (<140°C) compared to NAO brake temperatures (<120°C) is only about 20°C at most. The maximum brake disc temperature recorded using a brake assembly during an interlaboratory event varied over a wide range of 150–190°C [34]. We consider the maximum temperature of 120°C for NAO and 140°C for ECE in this study to be the maximum brake temperatures among the eight laboratories. Depending on the roughness of the pad surface, the real contact area may be much smaller than the apparent contact area, and the flash temperature of the real contact parts could exceed 1100°C [35–39]. Therefore, it is difficult to fully explain the mechanism based on only the bulk temperature. The formation of brake-wear particles is known to be caused by a very complex mechanochemical process that includes multiple compounds in the friction material [4].

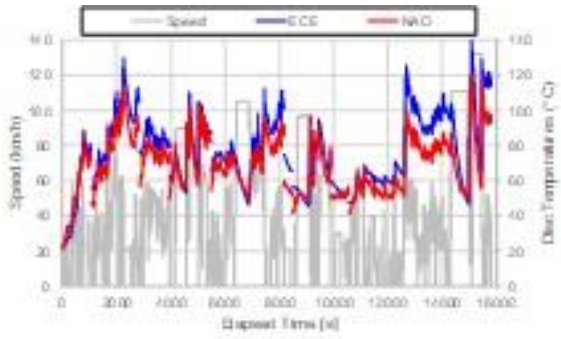

Figure 6. Temporal profiles of brake temperatures for NAO and ECE paired with conventional gray cast iron ventilated discs for the front brake axle.

We considered that the phase transformation from goethite (α-Fe(O)OH, Fe (III)) to iron oxides Fe_2O_3 (hematite (α-Fe_2O_3, Fe (III)) and Maghemite (γ-Fe_2O_3, Fe (III))) in the ECE brake in this study was due to a tribological reaction involving hydrothermal transformation [33] related to the above-mentioned differences in brake temperature and disc surface microstructure friction material. Because FeO can exist stably in the Fe-O phase transformation diagram at 700°C, we hypothesized that goethite (α-Fe(O)OH, Fe (III)) underwent a phase transformation to FeO via the formation of hematite (α-Fe_2O_3, Fe (III)), Maghemite (γ-Fe_2O_3, Fe (III)) and magnetite (Fe_3O_4, Fe (II, III)) by dehydrogenation. We suggest that the dehydrogenative phase transformation from goethite (α-Fe(O)OH, Fe (III)) to wüstite (FeO, Fe (II)) therefore resulted in a higher proportion of wüstite (FeO, Fe (II)), compared to NAO in the ECE brake. Even if the mechanism of corrosion and hydroxide

Preprints (www.preprints.org) | NOT PEER-REVIEWED | Posted: 13 December 2023 doi:10.20944/preprints202312.0786.v1

formation on the pad and iron surface due to moisture generated from organic matter in NAO is the main mechanism and hydroxide formation due to phase transition is the minor mechanism, the difference in observed iron oxides by NAO and ECE at the similar level of Fe content is a step toward meeting our goal.

3.2.5. Tribo-Reduction

One other feature of the results in Figure 5 is that the difference between NAO and ECE is that metallic Fe (α-Fe, Fe (0)) contributed less to ECE than to NAO. We often consider the generation of metallic iron (α -Fe, Fe (0)) by only abrasive wear from brake pads and cast iron discs [4,5]. We should also note that metallic Fe is also produced by tribo-chemical reduction with magnetite (Fe_3O_4, Fe (II, III)) as the starting material [40]. The following two reduction processes are required to produce metallic iron (α-Fe, Fe (0)) [40]. The reduction processes from magnetite (Fe_3O_4, Fe (II, III)) to wüstite (FeO, Fe (II)) occurs as follows:

$$Fe_3O_4 + CO \rightarrow 3Fe + CO_2\uparrow \quad (4)$$

$$Fe_3O_4 + H_2 \rightarrow 3FeO + H_2O\uparrow. \quad (5)$$

The reduction processes from wüstite (FeO, Fe (II)) to metallic iron (α-Fe, Fe (0)) then proceeds as follows:

$$FeO + CO \rightarrow Fe + CO_2\uparrow \quad (6)$$

$$FeO + H_2 \rightarrow Fe + H_2O\uparrow. \quad (7)$$

The reduction gases such as carbon monoxide (CO) and hydrogen (H_2) are generated by the decomposition of phenolic resin, which is a binder of brake pads [36,37,41–43], and the reduction processes can proceed as described in Equations (4)–(7) [40].

3.2.6. Tribo-Oxidations

The amount of magnetite (Fe_3O_4, Fe (II, III)) in brake-wear particles was higher in ECE than in NAO (Figure 5). Because of the small fraction of Fe (α-Fe, Fe (0)) and wüstite (FeO, Fe (II)) in NAO, the formation of Fe (α-Fe, Fe (0)) and wüstite (FeO, Fe (II)) from magnetite (Fe_3O_4, Fe (II, III)) by the tribo-reduction process in Equations (4)–(7) [40], which requires phenolic resin to be present on the pad and disc surfaces, does not follow. Under NAO pad-pairing conditions, the main iron oxides are hematite (α-Fe_2O_3, Fe (III)) and Maghemite (γ-Fe_2O_3, Fe (III)), which are produced mainly from the tribo-oxidation of the cast iron disc, in agreement with literature results [44,45], which predict a highly oxidative environment for this type of NAO pad tribological systems. The formation of magnetite (Fe_3O_4, Fe(II,III)) with a flash temperature (e.g., phase transformation temperature) of >586°C [32,33], would be less favored than the formation of hematite (α-Fe_2O_3, Fe (III)) and Maghemite (γ-Fe_2O_3, Fe (III)) [32,33]. In contrast, iron oxides (hematite (α-Fe_2O_3, Fe (III)) and Maghemite (γ-Fe_2O_3, Fe (III))) are produced by a mechanism involving a reaction of the brake-wear particles on the surface of the pad and disc with the outer atmosphere. However, at the time of the experiment, it was not possible to determine the detailed mechanisms for the formation of the main iron oxide (hematite (α-Fe_2O_3, Fe (III)) and Maghemite (γ-Fe_2O_3, Fe (III))) from the NAO and the smaller percentages of magnetite (Fe_3O_4, Fe (II, III)) in NAO rather than ECE. Further experiments will be required to identify these mechanisms.

4. Conclusions

In this study, we characterized the possible contribution of iron oxides and hydroxides to the airborne brake-wear particles under realistic vehicle driving and braking conditions with different friction materials. The conclusions of this study were as follows:

- Significant differences in wear coefficients and PM_{10} emissions were observed between NAO and ECE brake pads. Mass losses as wear factors were found to be 4.02 mg/km per brake for

the NAO pads and 9.31 mg/km per brake for the ECE pads. Emissions of brake-wear particles were 1.43 ± 0.29 mg/km per brake for PM_{10} with NAO and in 3.73 ± 0.19 mg/km per brake for PM_{10} with ECE.

- The dominant contribution to PM_{10} and $PM_{2.5}$ brake-wear particles was Fe for both NAO and ECE. The iron concentration ratio in the particle mass were comparable to the disc to pads ratio measured by wear mass.
- Differences in the consistency of iron oxides and hydroxides were observed between NAO and ECE brake pads.
- The hydroxide goethite (α-Fe(O)OH, Fe (III)) was detected only in the NAO pad. It is difficult to fully explain the mechanism based on only the bulk temperature, but a high goethite (α-Fe(O)OH, Fe (III)) contribution in the NOA brake was suggested because of the phase transformation from goethite (α-Fe(O)OH, Fe (III)) to iron oxides Fe_2O_3 (hematite (α-Fe_2O_3, Fe (III)) and Maghemite (γ-Fe_2O_3, Fe (III))) in this study.
- Metallic iron (α -Fe, Fe (0)) was generated not only from abrasive wear but also from the tribo-chemical reduction with magnetite (Fe_3O_4, Fe (II, III)) as the starting material.
- Magnetite (Fe_3O_4, Fe (II, III)), which is of interest from the point of view of health effects, was less abundant in NAO than in ECE. The implication is that magnetite (Fe_3O_4, Fe (II, III)) is less likely to form in NAO due to tribo-oxidations.

The quantification of iron speciation in this study could serve as an example of source identification in atmospheric observations of brake-wear particles and contribute to further research.

Author Contributions: Conceptualization, H.H.; methodology, H.H.; formal analysis, H.H., A.I. and T.O.; investigation, H.H., A.I. and T.O.; resources, H.H. and T.O.; data curation, H.H., A.I. and T.O.; writing—original draft preparation, H.H; writing—review and editing, H.H., A.I. and T.O.; visualization, H.H.; supervision, H.H., A.I. and T.O.; project administration, H.H.; funding acquisition, H.H., A.I. and T.O. All authors have read and agreed to the published version of the manuscript.

Funding: This work was partially supported by the Japan Society for the Promotion of Science (JSPS) KAKENHI Grant Number JP 22K03895 and JST CREST (JPMJCR19H3). The XAFS experiments were carried out at beamline 11 and 12 of SAGA-LS (project numbers: 1712126T, 1712131P, 1805035F, 1809080F, 1809081F, 1901140F, 1905032F).

Institutional Review Board Statement: Not applicable.

Informed Consent Statement: Not applicable.

Data Availability Statement: Only brake emission data presented in this study are available on request from the corresponding author. The data are not publicly available due to a confidentiality agreement with the part providers.

Acknowledgments: The author would like to thank co-workers who supported the set-up and operation of the dynamometer and the measurements. Dr. Hiroyuki Setoyama of the Kyushu Synchrotron Radiation Research Centre (SAGA-LS) helped with the acquisition and analysis of the XAFS spectra. The experiments using synchrotron radiation were performed at the beamlines BL11 and BL15 of the SAGA Light Source with the proposal Nos. 1809080F and 1809081F (for BL11), and also 22050540F and 2210101F (for BL15).

Conflicts of Interest: Not applicable.

References

1. WHO. Ambient Air Pollution: A Global Assessment of Exposure and Burden of Disease; World Health Organization: Geneva, Switzerland, 2016; p 131.
2. Beddows, D. C. S.; Harrison, R. M. PM_{10} and $PM_{2.5}$ Emission Factors for Non-Exhaust Particles from Road Vehicles: Dependence upon Vehicle Mass and Implications for Battery Electric Vehicles. *Atmos. Environ.* **2021**, 244. 117886. https://doi.org/10.1016/j.atmosenv.2020.117886
3. Pattammattel, A.; Leppert, V. J.; Aronstein, P.; Robinson, M.; Mousavi, A.; Sioutas, C.; Forman, H. J.; O'Day, P. A. Iron speciation in particulate matter (PM2.5) from urban Los Angeles using spectro-microscopy methods. *Atmos. Environ.* **2021**,245, 117988. https://doi.org/10.1016/j.atmosenv.2020.117988
4. Kukutschová, J.; Filip P. Chapter 6—Review of Brake-wear Emissions: a Review of Brake Emission Measurement Studies: Identification of Gaps and Future Needs. Amato, F. (Ed.), Non-Exhaust Emissions, Academic Press, **2018**, pp. 123-146. https://doi.org/10.1016/B978-0-12-811770-5.00006-6

5. Osterle, W.; Dmitriev, A. I. The role of solid lubricants for brake friction materials. *Lubricants* **2016**, 4, 22. https://doi.org/10.3390/lubricants4010005
6. Gonet, T.; Maher, B. A. Airborne, Vehicle-Derived Fe-Bearing Nanoparticles in the Urban Environment: A Review. *Environ. Sci. Technol.* **2019**, 53, 9970−9991. https://doi.org/10.1021/acs.est.9b01505
7. Gonet, T.; Maher, B.A.; Nyirő-Kósa, I.; Pósfai, M.; Vaculík, M.; Kukutschová. J. Size-resolved, Quantitative Evaluation of the Magnetic Mineralogy of Airborne Brake-Wear Particulate Emissions. *Environ. Pollut*. **2021**, 288, 117808. https://doi.org/10.1016/j.envpol.2021.117808
8. Nyirő-Kósa, I.; Ahmad, F.; Hoffer, A.; Pósfai, M. Nanoscale Physical and Chemical Properties of Individual Airborne Magnetic Particles from Vehicle Emissions. *Atmos. Environ. X* **2022**, 15, 100181. https://doi.org/10.1016/j.aeaoa.2022.100181
9. Maher, B.A. Airborne Magnetite- and Iron-Rich Pollution Nanoparticles: Potential Neurotoxicants and Environmental Risk Factors for Neurodegenerative Disease, Including Alzheimer's Disease. *J. Alzheim. Dis.* **2019**, 71, 361–375. https://doi.org/10.3233/jad-190204
10. Gramstat, S.; Mertens, T.; Waninger, R.; Lugovyy, D. Impacts on Brake Particle Emission Testing. *Atmosphere* **2020**, 11, 1132. https://doi.org/10.3390/atmos11101132.
11. Österle, W.; Deutsch, C.; Gradt, T.; Orts-Gil, G.; Schneider, T.; & Dmitriev, A. I. Tribological screening tests for the selection of raw materials for automtive brake pad formulations. *Tribo. Int.* **2014**, 73, 148–155. https://doi.org/10.1016/j.triboint.2014.01.017
12. Filip, P.; Weiss, Z.; Rafaja, D. On Friction Layer Formation in Polymer Matrix Composite Materials for Brake Applications. *Wear* **2002**, 252, 189–198. https://doi.org/10.1016/S0043-1648(01)00873-0
13. Verma, P. C.; Menapace, L.; Bonfanti, A.; Ciudin, R.; Gialanella, S.; Straffelini, G. Braking Pad-Disc System: Wear Mechanism and Formation of Wear Fragments. *Wear* **2015**, 322–323, 251–258.
14. Mathissen, M.; Grochowicz, J.; Schmidt, C.; Vogt, R.; zum Hagen, F.H.F.; Grabiec, T.; Steven, H.; Grigoratos, T. A Novel Real-World Braking Cycle for Studying Brake Wear Particle Emissions. *Wear* **2018**, 414–415, 219–226. https://doi.org/10.1016/j.wear.2018.07.020
15. Jing, W.; Saito, K.; Okamoto, T.; Saito, H.; Sugimoto, K.; Nishita-Hara, C.; Hara, K.; Hayashi, M.; Hasegawa, S.; Okuda, T. Characterization of Elemental Composition and Valence State of Cyclone-collected Aerosol Particles Using EDXRF and XAFS at Three Sites in Japan. *Asian J. Atmos. Environ.* **2022**,16, 40–58. https://doi.org/10.5572/ajae.2021.137
16. Saito, K.; Okuda, T.; Hasegawa, S.; Nishita-Hara, C.; Hara, K.; Hayashi, M. (2020) Chemical Speciation of Chromium in Atmospheric Particulate Matter Collected with Cyclone by XAFS Method. J. Jpn. Soc. Atmos. Environ. 2020, 55, 27–33, (in Japanese with English Abstract). https://doi.org/10.11298/taiki.55.27
17. Hagino, H.; Oyama, M.; Sasaki, S. Laboratory Testing of Airborne Brake Wear Particle Emissions using a Dynamometer System under Urban City Driving Cycles. *Atmos. Environ.* **2016**, 131, 269–278. https://doi.org/10.1016/j.atmosenv.2016.02.014
18. JASO C470. Passenger car—Measurement Method for Brake Wear Particle Emissions. **2020**, Edition, March 31, 2020.
19. Mathissen, M.; Grochowicz, J.; Schmidt, C.; Vogt, R.; Zum Hagen, F.H.F.; Grabiec, T.; Steven, H.; Grigoratos, T. A Novel Real-World Braking Cycle for Studying Brake Wear Particle Emissions. *Wear* **2018**, 414–415, 219–226. https://doi.org/10.1016/j.wear.2018.07.020
20. GRPE-2023-4e Rev.V6. Clean-(PMP) Proposal to Amend ECE/TRANS/WP.29/GRPE/2023/4. Proposal for a New UN GTR on Laboratory Measurement of Brake Emissions for Light-Duty Vehicles. Available online: https://wiki.unece.org/download/attachments/172852339/GRPE-2023-4e%20Rev.V6.docx?api=v2 (accessed on 22 November 2022).
21. Rule, A.; Geyh, A.; Ramos-Bonilla, J. P.; Mihalic, J. N.; Margulies, J. D.; Polyak, L. M.; Kesavan, J.; Breysse, P. Design and Characterization of a Sequential Cyclone System for the Collection of Bulk Particulate Matter. *J. Environ. Monit.* **2010**, 12, 1807–1814. https://doi.org/10.1039/C0EM00034E
22. Okuda, T.; Isobe, R.; Nagai, Y.; Okahisa, S.; Funato, K. Inoue, K. Development of a High-Volume $PM_{2.5}$ Particle Sampler Using Impactor and Cyclone Techniques. *Aerosol Air Qual. Res.* **2015**. 15, 759–767. https://doi.org/10.4209/aaqr.2014.09.0194
23. Ishihara, N.; Okuda, T.; Hagino, H.; Oguro, A.; Tani, Y.; Okochi, H.; Tokoro, C.; Fujii-Kuriyama, Y.; Itoh, Vogel, C.F.A.; Ishihara, Y. Involvement of Polycyclic Aromatic Hydrocarbons and Endotoxin in Macrophage Expression of Interleukin-33 Induced by Exposure to Particulate Matter. *J. Toxicol. Sci.* **2022**, 47, 201–210. https://doi.org/10.2131/jts.47.201

24. Chow, J.C.; Watson, J.G.; Crow, D.; Lowenthal, D.H.; Merrifield, T. Comparison of IMPROVE and NIOSH Carbon Measurements. *Aerosol Sci. Technol.* **2001**, 34. 23–34. https://doi.org/10.1080/02786820119073
25. Spada, N.J.; Yatkin, S.; Giacomo, J.; Trzepla, K.; Hyslop, N.P. Evaluating IMPROVE $PM_{2.5}$ Element Measurements. *J. Air Waste Manag. Assoc.* **2023**, 73, 843–852. https://doi.org/10.1080/10962247.2023.2262417
26. Ravel, B.; Newville, M. ATHENA, ARTEMIS, HEPHAESTUS: data analysis for X-ray absorption spectroscopy using IFEFFIT. *J. Synchrotron Rad.* **2005**, 12, 537–541. doi:10.1107/S0909049505012719
27. Grigoratos, T.; Mathissen, M.; Vedula, R.; Mamakos, A.; Agudelo, C.; Gramstat, S.; Giechaskiel, B. Interlaboratory Study on Brake Particle Emissions—Part I: Particulate Matter Mass Emissions. *Atmosphere* **2023**, 14, 498. https://doi.org/10.3390/atmos14030498
28. Storch, L.; Hamatschek, C.; Hesse, D.; Feist, F.; Bachmann, T.; Eichler, P.; Grigoratos, T. Comprehensive Analysis of Current Primary Measures to Mitigate Brake Wear Particle Emissions from Light-Duty Vehicles. *Atmosphere* **2023**, 14, 712. https://doi.org/10.3390/atmos14040712
29. Hinds, W.C.; Yifang, Z. Chapter 4—Particle Size Statics: Aerosol Technology: Properties, Behavior, and Measurement of Airborne Particles, 3rd ed. John Wiley & Sons, Inc. **2022**, pp. 65-94. ISBN: 978-1-119-49406-5
30. Iijima, A.; Sato, K.; Yano, K.; Kato, M.; Kozawa, K.; Furuta, N. Emission Factor for Antimony in Brake Abrasion Dusts as One of the Major Atmospheric Antimony Sources. *Environ. Sci. Technol.* **2008**, 42, 8, 2937–2942. https://doi.org/10.1021/es702137g
31. Motta, M.; Fedrizzi, L.; Andreatta, F. Corrosion Stiction in Automotive Braking Systems. *Materials* **2023**, 16, 3710. https://doi.org/10.3390/ma16103710
32. Takada, T. Formation and Physical Properties of Iron Oxides Hydroxides, Review. *Denki Kagaku oyobi Kogyo Butsuri Kagaku* **1969**, 37, 328–335. (in Japanese with English Figures). https://doi.org/10.5796/kogyobutsurikagaku.37.328
33. Diamandescu, L.; Mihăilă-Tărăbăşanu, D.; Popescu-Pogrion, N. Hydrothermal Transformation of α-FeOOH into α-Fe_2O_3 in the Presence of Silicon Oxide. *Materials Lett.* **1996**, 27, 253–257. https://doi.org/10.1016/0167-577X(95)00295-2
34. Grigoratos, T.; Agudelo, C.; Grochowicz, J.; Gramstat, S.; Robere, M.; Perricone, G.; Sin, A.; Paulus, A.; Zessinger, M.; Hortet, A.; et al. Statistical Assessment and Temperature Study from the Interlaboratory Application of the WLTP–Brake Cycle. *Atmosphere* **2020**, 11, 1309. https://doi.org/10.3390/atmos11121309
35. Sutter, G.; Ranc, N. Flash Temperature Measurement during Dry Friction Process at High Sliding speed. *Wear* **2010**, 268, 1237–1242. https://doi.org/10.1016/j.wear.2010.01.019
36. Okayama, K.; Kishimoto, H.; Hiratsuka, K. Tribo-Reduction of Metal Oxides by Tribo-Degradation of Phenolic Resin in Brake Pad. *Trans. Jpn. Soc. Mech. Eng. C* **2013**, 79, 2558-2570 (in Japanese with English Figures). doi:10.1299/kikaic.79.2558
37. Lange, J.; Ostermeyer, G.; The Effect of Metal Pickup to the Friction Interfaces, *SAE Tech. Pap.* **2011**, 2011-01-2348, doi:10.4271/2011-01-2348
38. Kawamoto, M.; Shintani, S.; Sone, T.; Okabayashi, K. Wear Characteristics of Carbon Steel and 17Cr Stainless Steel in Relation to the Surface Temperature. *J. Japan Inst. Met. Mater.* **1973**, 37, 1236–1242 (in Japanese with English Figures), doi:10.2320/jinstmet1952.37.11_1236
39. Kawamoto, M.; Shintani, S.; Okabayashi, K. Relation between Wear of Iron and Steel and Sliding Surface Temperature. *Tetsu-to-Hagane* **1975**, 61, 3139–3148 (in Japanese with English Figures). doi:10.2355/tetsutohagane1955.61.15_3139
40. Noda, H.; Takei, T. Analysis of Metal Pick-Up Formation Process within Automotive Brake Pad. *SAE Int. J. Mater. Manf.* **2020**, 13, :27-43, https://doi.org/10.4271/05-13-01-0003
41. Nukumizu, K.; Kobayashi, T.; Abe, T.; Unno, M.. Study of the Formulation Mechanism for Metal Pick-up on the Frictional Surface of a Disc Brake Pad. *SAE Tech. Pap.* **2008**, 2008-01-2541. doi:10.4271/2008-01-2541.
42. Funabiki, K.; Nakamura, M.; Tsuriya, M. Carbonization of Phenolic Resins. *Jpn. Thermo. Plastic Ind. Assoc.* **1981**. 2, 220–235. doi:10.11364/networkpolymer1980.2.220
43. Inoue, M.; Hara, Y.; Sasada, T.; Degradation of Cured Phenolic Resin for Brake Lining Caused by Shearing Force: 1st Report, Molecular Weight Distribution of Extracts. *Trans. Jpn. Soc. Mech. Eng. C.* **1990**, 56, 222–227. doi:10.1299/kikaic.56.222

44. Straffelini, G.; Pellizzari, M.; Maines, L. Effect of Sliding Speed and Contact Pressure on The Oxidative Wear of Austempered Ductile Iron. *Wear* **2011**, 270, 714–719. https://doi.org/10.1016/j.wear.2011.02.004
45. Straffelini, G; Molinari, A. Mild Sliding Wear of Fe-0.2%C, Ti-6%Al and Al-7072: a Comparative Study. *Tribol. Lett.* 2011, 41. 227–238. https://doi.org/10.1007/s11249-010-9705-2